

Optimization model for endurance performance of electric rotorcraft transport drones and its application prospects

Huang Zihan, Long Bo, Li Jiyu

College of Engineering, South China Agricultural University, Guangzhou, China

Article Info

Article history:

Received Oct 6, 2024

Revised Jan 8, 2025

Accepted Jan 26, 2025

Keywords:

Endurance

Model

Optimization

Partition

Transport unmanned aerial vehicles

ABSTRACT

The operational parameter configuration and performance optimization of electric rotorcraft transport unmanned aerial vehicles (UAVs) currently lack comprehensive guiding theory, impacting UAV endurance and efficiency, thereby limiting industry growth. This paper analyzes factors affecting UAV endurance and establishes a hover endurance model for electric rotorcraft transport UAVs through theoretical derivation and testing. Based on this model, we introduce the concepts of thrust redundancy coefficient and load cut-off line, proposing an optimal endurance configuration theory. This theory categorizes the parameter configuration range into light load, ideal configuration, load cut-off, and endurance saturation zones. Using current operational parameters, we evaluate and optimize UAV performance. Verification results demonstrate high model accuracy, with error rates ranging from 1.89% to 5.69%. After optimization, the payload capacities of two transport UAVs increased by 6.25%, and their endurance improved by 6.97% and 9.5%, respectively, enhancing overall efficiency. This model provides a solid framework for assessing endurance capabilities and offers targeted optimization suggestions, making it crucial for improving UAV performance.

This is an open access article under the [CC BY-SA](https://creativecommons.org/licenses/by-sa/4.0/) license.



Corresponding Author:

Li Jiyu

College of Engineering, South China Agricultural University

Tianhe District, Guangzhou, Guangdong, China

Email: lijyu@scau.edu.cn

1. INTRODUCTION

The growing demand for logistics transportation has exposed the limitations of traditional human-powered delivery methods, which are not only time-consuming and labor-intensive but also pose safety risks like fatigue-related accidents. These limitations highlight the urgent need for more efficient alternatives. Compared to human-powered delivery methods, drone transport offers advantages such as rapid delivery, strong adaptability, high safety, and flexibility. These benefits make drone transport an important choice across various industries [1]–[4].

One of the significant challenges in deploying drones for logistics, however, is optimizing their endurance—the amount of time they can operate before needing to recharge or replace batteries. The central scientific problem addressed in this research is the optimization of endurance in electric transport unmanned aerial vehicles (UAVs), specifically focusing on the interactions between the power system, battery parameters, and operational load. By understanding how these factors collectively influence the overall endurance, this research provides critical insights for improving UAV operational efficiency, making them more viable for real-world logistics applications.

Currently, there are numerous models of drones on the market, each with significant performance differences, though their structural components are largely similar. In terms of the airframe, most drones use

modular designs for easy and quick maintenance and replacement. They extensively use lightweight and corrosion-resistant composite materials, which reduce the weight of the airframe and enhance adaptability to various environments. For power, high-power brushless motors are commonly used due to their simple and reliable structure and relatively low cost, facilitating large-scale production. Control systems often feature highly interference-resistant, redundant intelligent flight controllers combined with GPS/RTK positioning modules [5], enabling highly precise automated operations. For energy, lithium polymer batteries are used due to their strong instantaneous discharge capability, meeting the high-power output demands of the motors. However, the low energy density of lithium batteries prevents long-duration high-current discharge, resulting in generally low endurance times for drones and limiting their operational performance [6], [7]. Increasing battery capacity can enhance endurance to some extent, but excessive battery weight leads to additional energy consumption. The operational load determines the continuous working capability of electric rotorcraft UAVs and must be reasonably matched with endurance time to achieve optimal continuous operation. The power system, comprising motors, electronic speed controllers (ESCs), and propellers, determines the overall operational output power of the UAV, significantly impacting its endurance capabilities. In summary, the endurance of transport drones is mainly influenced by the power system, battery parameters, and operational load. Effective improvement of drone endurance and operational efficiency under current technological conditions relies on the optimal matching of these three components.

Current research related to UAV endurance optimization mainly focuses on the optimization of the fuselage structure layout and the parameter matching the power system. Zhan *et al.* [8] studied the effect of multi-wing single-arm tandem layout electric UAV rotor spacing on energy consumption, and through experiments, they obtained the best rotor spacing under different layouts. However, the impact of changes in the fuselage configuration on the test results was not considered; Yang [9] used Fluent software to optimize the parameters of a single rotor. Zhang and Xie [10] used momentum leaf element theory and considered the effect of viscosity to optimize the structural parameters of the blade. Both methods effectively improve the rotor pull coefficient but only consider the impact of the UAV power system, which has a limited effect on the efficiency of the whole aircraft. Liu and Ma [11] used genetic optimization algorithms to multitarget UAV body parameters. Zhang and Liu [12] proposed optimization, which is a specific method for improving the endurance of electric rotary-wing UAVs; however, this method does not consider the impact of load changes on the endurance time and is only applicable when UAVs do not carry a payload. Combining the traditional multirotor UAV with the helicopter rotor structure effectively improves the load capacity and flight stability of six-rotor UAVs. Duan *et al.* [13] proposed a BP neural network algorithm based on the beetle algorithm. The power optimization control strategy of the variable-pitch electric power system can obtain the best combination of rotor speed and pitch, which proves the performance advantages of the new variable-pitch rotor structure. However, the related research results are not applicable to conventional electric UAVs and have limited practical guidance value.

In summary, current research on optimizing the endurance of electric multi-rotor transport drones primarily focuses on the impact of individual parameters on overall flight time. However, this study finds that optimal endurance performance can only be achieved through the coordinated optimization of the UAV's power system, battery configuration, and operational load. Adjusting the parameters of individual modules has limited impact on the overall system, as the configurations of different components can interact and influence operational performance [14]–[17]. Only by considering the interactions among these factors can optimal endurance be realized. Therefore, understanding the patterns of endurance time variation is critical, and a holistic assessment of the drone's overall endurance performance is necessary. This approach allows for targeted optimization and upgrade recommendations, ultimately enhancing the operational efficiency of transport drones.

This study focuses on electric transport drones as the primary research object. By maintaining a fixed frame structure, we conducted theoretical derivations based on the operational principles of key components, including the power system, battery configuration, and payload design. These derivations culminated in the development of an endurance calculation model, enabling a systematic evaluation of drone endurance under varying operational scenarios. To validate the accuracy of the model, field experiments were conducted at seven validation points, testing the endurance of the drone under different configurations and comparing the results with theoretical values. Through the analysis and discussion of the model images, the configuration characteristics of each endurance area are summarized, and a set of targeted transport UAVs operation efficiency optimization theories is extracted. The model and regularity can be used to obtain the optimal adaptation scheme between the transport UAVs battery and the operating load, improve the endurance of UAVs, and increase the operation efficiency. It also has a certain guiding significance for the design and optimization of transport UAVs. Optimizing drone endurance will significantly improve transportation efficiency, reduce costs, and promote wider adoption in logistics, especially in express delivery

and remote areas. It also helps reduce reliance on traditional methods, alleviating traffic congestion and lowering carbon emissions, benefiting environmental protection.

2. THE COMPREHENSIVE THEORETICAL BASIS

2.1. Electric rotor transport UAVs endurance model

In actual field flight operations, the endurance of transport UAVs is affected by many factors [18], [19]. To simplify the structure of the model in this paper, transport UAVs are taken in the hovering state as the main research object. The factors affecting its endurance include take-off quality, number of rotors, and total battery energy. Among them, the take-off mass is composed of the empty aircraft mass W_1 , payload mass W_2 , and battery mass W_3 . The total pulling force of the motor in the hovering state is equal to the take-off mass. For a UAV with n rotors, the single-motor pull T can be regarded as $1/n$ of the take-off mass; that is

$$T = \frac{W_1 + W_2 + W_3}{n} \quad (1)$$

If the motor pull changes, the total output power of the UAV will change accordingly, which will affect the endurance time. When the brushless motor is working, the corresponding relationship between the output pull and the output power can be represented by a curve. With the help of the manufacturer's force efficiency test data in the motor technical parameter manual, through polynomial fitting, the corresponding fitting function $P(T)$ of the motor pull and power can be calculated, and then the motor output power under different pulls can be accurately obtained. The power of each motor is accumulated and summed, and the result is the output power of the power system. In the hovering power distribution system of electric rotor UAVs, the motor power of the power system accounts for 90% [20]. After adding the power compensation coefficient K (according to the power ratio relationship, the value is 1.1), 110% of the output power of the power system can be approximated as the total hovering output power of the UAV. Combined with the discharge law of lithium batteries [21]–[24], in the uniform discharge state, the discharge time of the UAV battery is the endurance time t , which is composed of the battery energy W , the number of rotors n , and the hovering output power of a single motor $P(T)$. The relationship between these three parameters is as follows:

$$t = \frac{W_3 \cdot e}{1.1n \cdot P(T)} \quad (2)$$

where e is the energy density of the battery, and the product of the energy density and the mass of the battery is the total energy of the battery.

In summary, (1) and (2) are the theoretical calculation model of the hovering lifetime of electric rotary-wing transport UAVs. The input parameters of the model include battery quality, battery energy density, payload quality, empty aircraft quality and motor thrust fitting function. Moreover, the output parameter is the hovering endurance time. This model can calculate the hovering endurance time under different parameter configurations in combination with specific model parameters, providing a theoretical basis for the endurance evaluation and analysis of transport UAVs.

2.2. Model analysis and regularity

2.2.1. Endurance model analysis

To cope with extreme working conditions, a transport UAVs needs to have a certain power redundancy [25]. When the UAV is flying horizontally and at a constant speed, the angle between the motor's pulling force axis and the fuselage's gravity axis is θ , as shown in Figure 1. As the flight speed increases, the included angle gradually increases. At this time, the motor needs to increase the pulling force output to maintain the force balance in a vertical direction and ensure that the flight height remains unchanged. If the tilt angle is too large or the motor output pull is insufficient, it will cause the UAV to lose altitude and threaten flight safety. Taking the Pixhawk flight controller as an example, the maximum flight angle of the UAV is set in the flight controller defaults at 45° . This means that when the inclination of the fuselage reaches 45° , the UAV can still maintain horizontal flight to ensure flight safety. At this time, the ratio of the vertical component of the motor pull to the total motor pull is the pull redundancy coefficient η . The calculation shows that when the inclination angle of the fuselage is 45° , the power redundancy coefficient η is taken as 0.707. The relationship between the maximum take-off mass WT and the maximum thrust of the motor T_{max} .

$$W_T = \eta \cdot n \cdot T_{max} \quad (3)$$

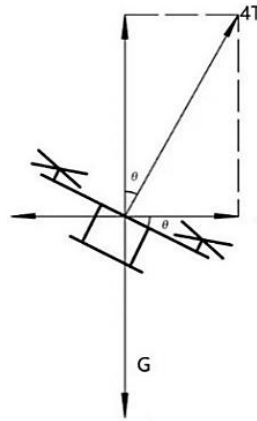


Figure 1. Force analysis of UAVs

In fact, the current value of the pulling force redundancy coefficient can only meet the basic safety requirements of transport UAVs. If the relevant parameters are configured according to the maximum load capacity, transport UAVs are prone to body structure fatigue deformation [26], motor overheating demagnetization [27] and other adverse consequences during long-term, heavy-load and high-frequency use, which shortens the life of the product. Therefore, in the product design stage of transport UAVs, relevant manufacturers, will appropriately reduce the redundancy factor, improve the operating conditions of airborne equipment, and extend the service life. The power redundancy coefficients of some mainstream transport UAVs are shown in Table 1.

Table 1. Pull force redundancy coefficient of mainstream transport UAVs

Model	Motor	Maximum motor pull (N)	Rotor number	Maximum take-off mass (kg)	Pull force redundancy factor
DJI MG1P	6010	58.8	8	24.8	0.689
DJI T20	10015	132.3	6	47.5	0.586
XAG P20	A12	151.9	4	32	0.516
XAG P30	A16	191.1	4	41	0.526
XAG P40	A25	196	4	48	0.6

Table 1 shows that the dynamic redundancy coefficient of mainstream transport UAVs varies from 0.516 to 0.689. To take into account both the operational efficiency and the flight stability, 0.5 is used here as the lowest redundancy factor. In summary, the setting change range of the pulling force redundancy coefficient is 0.5~0.707. When the value of the redundancy coefficient is close to 0.707, the load capacity of the whole machine is stronger, and the operation efficiency is improved. However, the service life of the machine body is shortened. When the value of the redundancy coefficient is close to 0.5, the service life of the whole machine is prolonged, but the load capacity is weakened, and the operation efficiency is reduced.

To further analyze the theoretical model of endurance, the AX-1000 UAV is taken as an example. Its main performance parameters are shown in Table 2. The pull-power fitting function $P(T)$ of the standard motor is $y = 15.01x^2 + 70.01x - 3.936$ ($R^2 = 0.996$), and the maximum motor pull is 58.8 N.

Table 2. Performance parameters of the AX-1000 UAV

Frame size (cm)	Flight control model	Motor	ESC	Blade	Aircraft mass (kg)	Standard load (kg)	Flying speed (m/s)
80*80*40	DJI A3	Sunnysky 6215	100A	22*6.6	5	5	0~9

Substituting the above parameters into the model, the resulting model image is shown in Figure 2(a). Combining Table 1 and (3), it can be seen that when the power redundancy factor is 0.707, the maximum take-off mass of the UAV is 17 kg, and the maximum load capacity after removing the empty aircraft mass is 12 kg. The corresponding battery and workload configuration area is triangular, and the regional boundary expression is (4).

$$x + y \leq 12 \tag{4}$$

Combining the theoretical model of endurance time and the motor pull-power fitting curve shown in Figure 2(b), it can be seen that when the UAV is hovering, each motor pull operating point corresponds to a constant load state. Moreover, under constant load, the hovering output power is basically constant, and the endurance time increases proportionally with an increasing battery mass in the total load. Thus, the endurance change line corresponding to the constant load is a straight line in space. As the constant load increases, the operating point of the motor pulling force increases, and the slope of the corresponding endurance change line gradually becomes larger, as shown in the 4x19.6/29.4/39.2 N pulling force corresponding to the endurance change line in Figure 2(a).

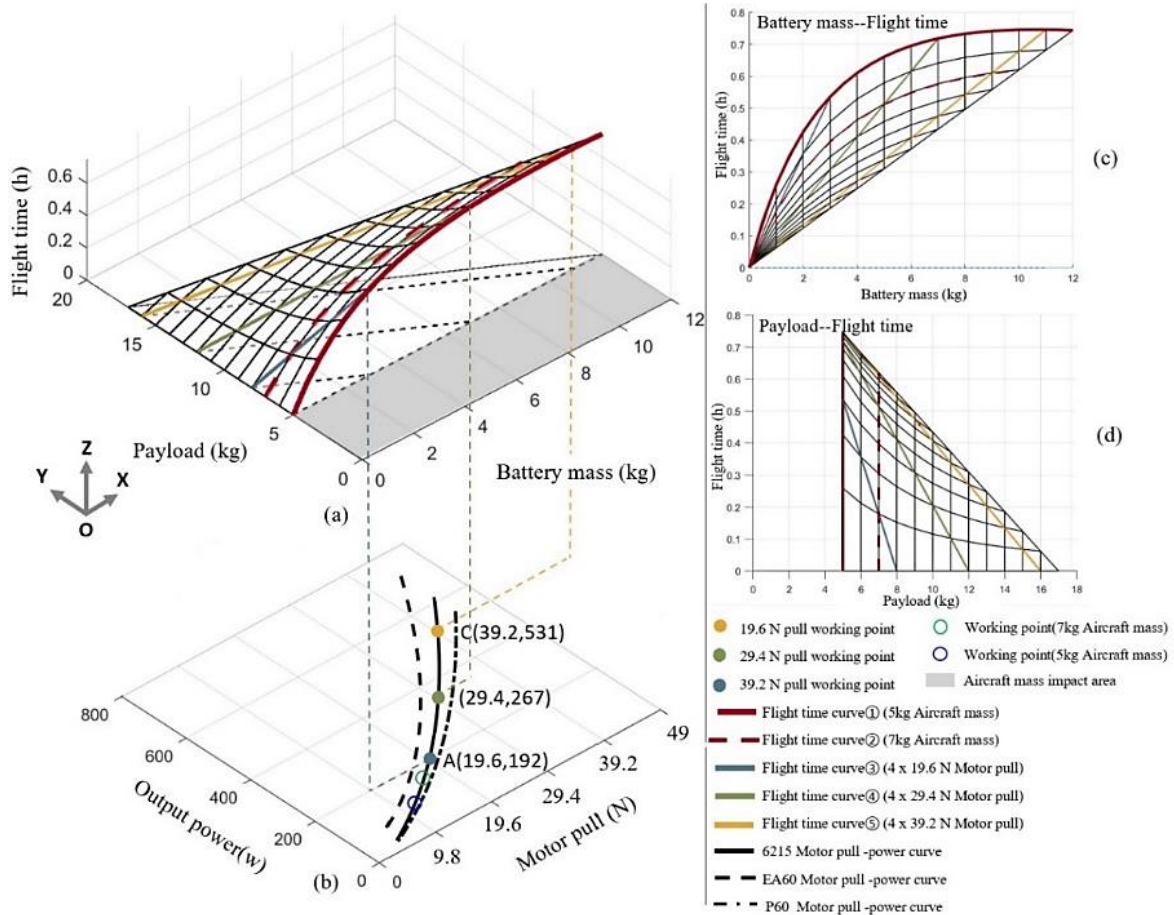


Figure 2. Image of the endurance model (a) the resulting model image (b) motor pull-power fitting curve (c) front view of the endurance surface (d) the left side view of the endurance surface

In addition to the battery and payload configuration, the shape of the model is also affected by the mass of the empty aircraft, the battery energy density and the motor pull-power fitting curve. Among them, the effect of the change in the quality of the empty aircraft on the endurance time is similar to the payload, so the quality of the empty aircraft can be equivalent to the payload, which is represented by the blank payload change area of 0-5 kg in Figure 2(a). If the mass of the empty aircraft increases by 2 kg, the output pulling force corresponding to the working point of the motor pulling force will be increased from 12.25 N to 17.15 N, and the endurance curved surface will shift to the inside of the curved surface. The configuration space between the battery and the payload will be further compressed, and aircraft performance will decline. The load capacity is reduced from 12 kg to 10 kg, and the maximum endurance time is reduced from 0.745 h to 0.629 h. The battery energy density only changes the absolute value of the endurance surface without changing the shape of the surface. If a battery with a higher energy density is used, the entire endurance surface will shift upward, and the amount of translation is proportional to the increase in battery energy density. When the motor or rotor is replaced, that is, when the motor pull-power fitting curve changes, the

endurance surface shape changes, and the pulling force operating point will also move to the new motor fitting curve. The tensile force of the new operating point remains unchanged, but the corresponding output power changes, as shown by the dashed line in Figure 2(b).

2.2.2. Optimal endurance configuration regularity

Figure 2(c) is a front view of the endurance surface, reflecting the influence of battery quality on the endurance. Based on this result, the corresponding curve of the endurance time of the UAV with the battery quality under different payloads (represented by different life curves in the figure) is drawn, as shown in Figure 3(a). It can be seen from the figure that the effect of increasing the mass of the battery on the endurance time decreases with the improvement of the take-off quality. After the endurance turning point is reached, continuing to increase the battery will cause the endurance to deteriorate. The reason for the above phenomenon is that after the take-off mass increases, the motor pulling force increases accordingly, and the corresponding output power growth rate is higher than the battery energy growth rate, which ultimately leads to a reduction in the endurance time. In the load range of 0-12 kg, as the payload increases, the maximum endurance time decreases, and the endurance curve in the figure shows an overall downward trend. Combined with the motor pull-power fitting curve shown in Figure 2(b), it can be seen that when the motor pull change is the same, the power change in the high-pull area is significantly higher than that in the low-pull area, and the corresponding high-load area has a more significant decrease in the endurance time.

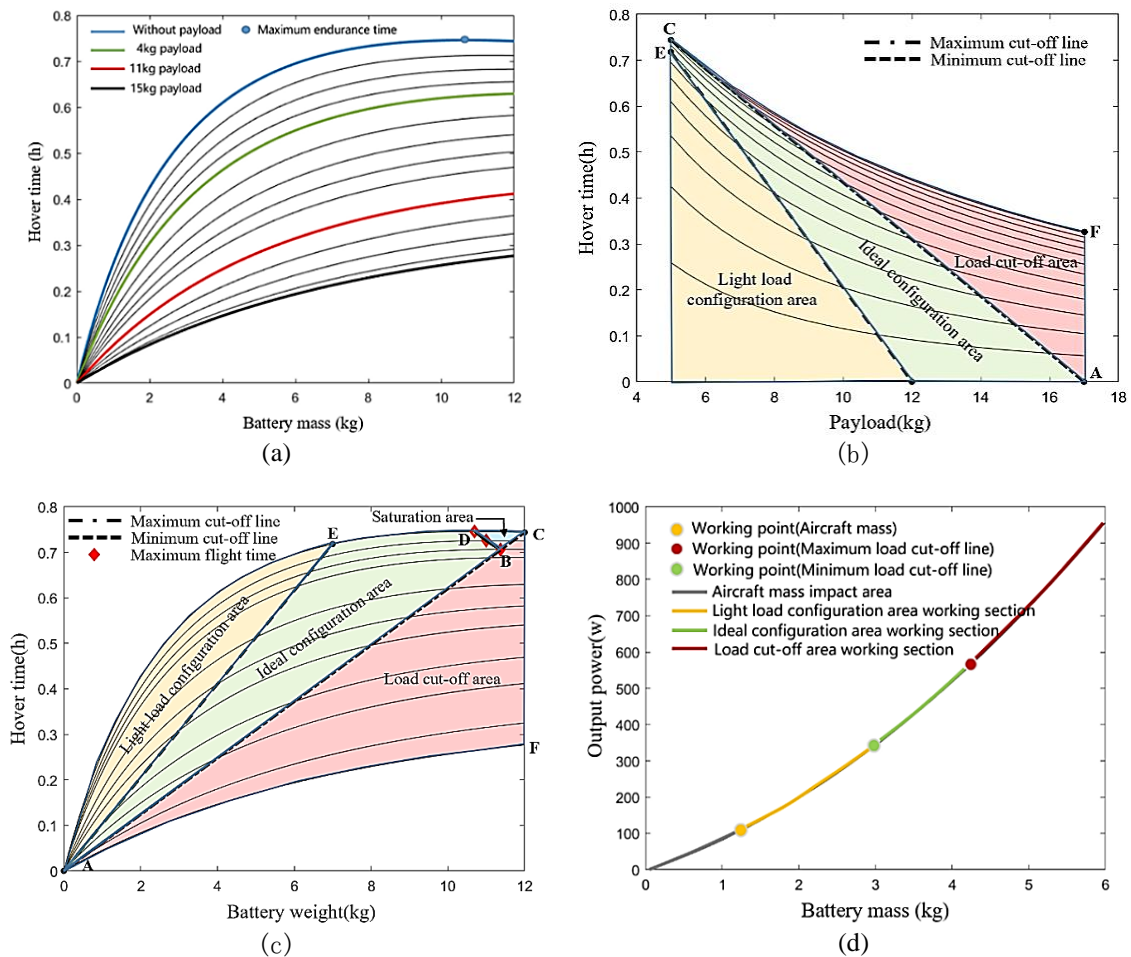


Figure 3. Analysis diagram of the battery life configuration (a) battery life curve, (b) left view endurance area division, (c) front view endurance area division, and (d) motor pull-power fitting curve

The endurance change curve in Figure 3(a) forms a closed plane. The upper boundary of the plane is composed of curve segments AE and EC, which represent the unloaded endurance change curve of the UAV. The highest point D of the boundary curve is the maximum endurance time; boundary CF and boundary AF

correspond to the endurance of the UAV at the maximum battery and payload, respectively. To divide the plane, the concept of the tensile redundancy coefficient is introduced, and the maximum/minimum redundancy coefficient can be calculated in combination with (3). The load mass is 5 kg/12 kg. If the maximum load configuration points of all the endurance curves are connected, the load cut-off line can be formed. When the payload reaches the maximum value, the corresponding battery quality is 0; thus, the load cut-off line passes through the zero point of the coordinate axis. The slope of the endurance line is determined by the hovering output power under the corresponding load, and its expression is

$$k = \frac{1}{n \cdot P(T_{\max})} \quad (5)$$

For a transport UAVs of a given configuration, the maximum motor pull and the pull-power fitting function are both quantitative. Therefore, after selecting the power redundancy coefficient, the slope of the cut-off line is determined immediately, and there is a unique load cut-off line corresponding to it. Only when the transport UAVs changes its power configuration and the corresponding relationship between the maximum motor pull T_{\max} and the output power $P(T)$ changes, does the slope k change accordingly.

The load cut-off lines AE and AC in Figure 3(c) divide the endurance plane into three areas with different areas. Below AC is the load cut-off area. The configuration parameters of this area exceed the take-off mass limit and have no practical application value. The area between AC and AE is an ideal configuration area. The configuration parameters in this area highlight the load capacity of transport UAVs under the premise of ensuring flight safety. It carries more payload and batteries and achieves higher operating efficiency. Appropriate parameter configuration points can be selected according to product requirements; above the AE is the light-load configuration area, the load in this area is low, and it is not suitable for the operation parameter configuration of transport UAVs. However, for light-load UAVs, the light-load configuration area is the ideal configuration area. The parameters in this area can provide a theoretical basis for the optimization of the endurance of light-load models such as remote sensing and surveying. The theoretical expressions of the above regions are (6).

$$\begin{cases} k \leq 4 \cdot P_{(0.5T_{\max})} & (\text{Load cut-off area}) \\ 4 \cdot P_{(0.5T_{\max})} \leq k \leq 4 \cdot P_{(0.707T_{\max})} & (\text{Ideal configuration area}) \\ k \geq 4 \cdot P_{(0.707T_{\max})} & (\text{Light-load configuration area}) \end{cases} \quad (6)$$

In the ideal configuration area, most of the endurance curves increase monotonically with the increase in the battery, and the maximum battery mass is the longest endurance configuration. However, for some models, when the payload is lower than a certain value, the endurance point no longer corresponds to the maximum battery quality. Continuing to increase the battery on the basis of the extreme point will cause the endurance of transport UAVs to deteriorate. After connecting these extreme points of endurance in series, the curve DB formed is a parabola with an opening upward, and its expression is,

$$y = ax^2 + bx + c \quad (7)$$

The curve DB intersects the maximum load cut-off line AC and the no-load endurance curve AEDC. The closed area formed is the endurance saturation zone. The endurance time in this area decreases with the improvement of battery quality. After the saturation zone is determined, the curve ABD formed by the area boundary BD and the maximum load cut-off line AC is the optimal endurance configuration line of the endurance configuration area. The configuration line contains the longest UAV endurance configuration point under any payload. In practical applications, to achieve the longest endurance time, the operating parameter configuration point should fall on the optimal endurance configuration line ABD; to take into account endurance and operating stability, when setting transport UAV operating parameters, appropriate configuration parameters should be selected in the ideal configuration area according to actual operational requirements.

Figure 2(d) is the left side view of the endurance surface, reflecting the influence of the payload on the endurance time. Based on this, the corresponding curve of the endurance time of the UAV under different battery configurations (represented by different endurance curves in the figure) is drawn as a function of the load quality of the operation, and the result is shown in Figure 3(b). It can be seen from this figure that when the battery increase is the same, the endurance of the low-load area is improved more significantly; the two load cut-off lines divide the entire configuration area into three areas, and the configuration characteristics of each area are the same as in Figure 3(c). Since the figure cannot reflect the existence of the endurance saturation zone, its regional distribution characteristics are for reference only. In the subsequent model application evaluation, the corresponding partition regularity of the front view of the endurance surface is used as the benchmark.

The area division boundaries in Figures 3(b) and 3(c) are all related to the motor pull curve, and their corresponding relations are all marked in Figure 3(d). Figure 3(d) shows that the light-load configuration zone, ideal configuration zone, and load cut-off zone essentially correspond to the light-load working section, medium-load working section, and heavy-duty working section of the motor pull-power fitting curve. At the end of the medium load working section that is close to the heavy-duty working section, the operating efficiency of transport UAVs can reach the highest level under the premise of ensuring flight safety.

3. METHOD

3.1. Verification point selection

The main conclusions of the existing UAV endurance configuration plane partition regularity include i) the total load remains unchanged, and the rate of change in the mass of the battery is equal to the rate of change in endurance time; ii) when configuring parameters and changing the battery and payload at the same time, the endurance time can remain unchanged; and iii) there is a turning point in the curve corresponding to the change in the endurance time with the battery mass, and there is a saturation zone in the endurance configuration plane.

To verify the accuracy of the above conclusions and to examine the accuracy of the model at the same time, the distribution of the selected verification points ①~⑦ on the existing endurance configuration plane is shown in Figure 4.

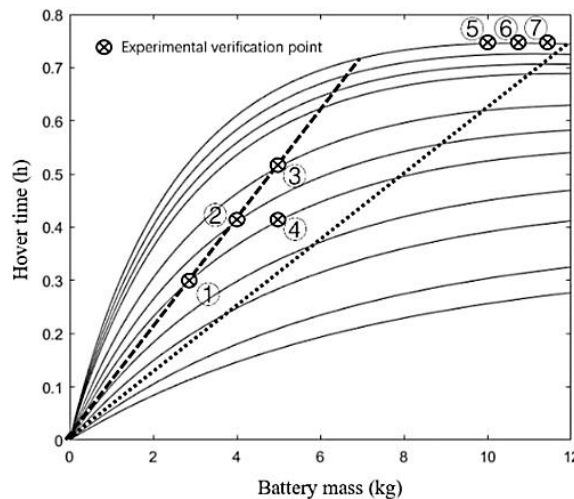


Figure 4. Distribution of the verification points

3.2. Experimental equipment

The experimental model is an AX-1000 rotary-wing transport UAVs. Its fuselage structure is shown in Figure 5. To obtain the output power data during the hovering process of the transport UAVs, the research team selected the ZFT-8 curve power meter as the auxiliary measurement equipment. The relevant parameters are shown in Table 3. The power meter includes a power interface, which is connected in series with the main circuit of the UAV during operation and can record the current, voltage and power data during the battery discharge process in real time and store it inside the device. After the test is completed, the data can be sent to the computer in the form of an xls-file through the host computer, which is convenient for subsequent data processing and analysis.

3.3. Calculation method of the endurance time

Due to the differences in the discharge performance of different batteries, even if the discharge power remains the same, the discharge time of the batteries of the same specification will not be the same. To reduce the experimental error, the verification experiment adopts the equivalent endurance time calculation method to calculate the hovering time as follows. After obtaining the hovering output power of the UAV in different configurations through the curved power meter, the stable is selected for 3 minutes. The data are outputted, the average output power $P(T)$, is calculated and then the total battery energy E is obtained according to the battery parameters. The final equivalent endurance time t is

$$t = \frac{E}{P(T)} \quad (8)$$

After applying this method to the model calculation and the endurance time extraction in the verification experiment, the performance difference between the individual batteries no longer affects the model verification results.

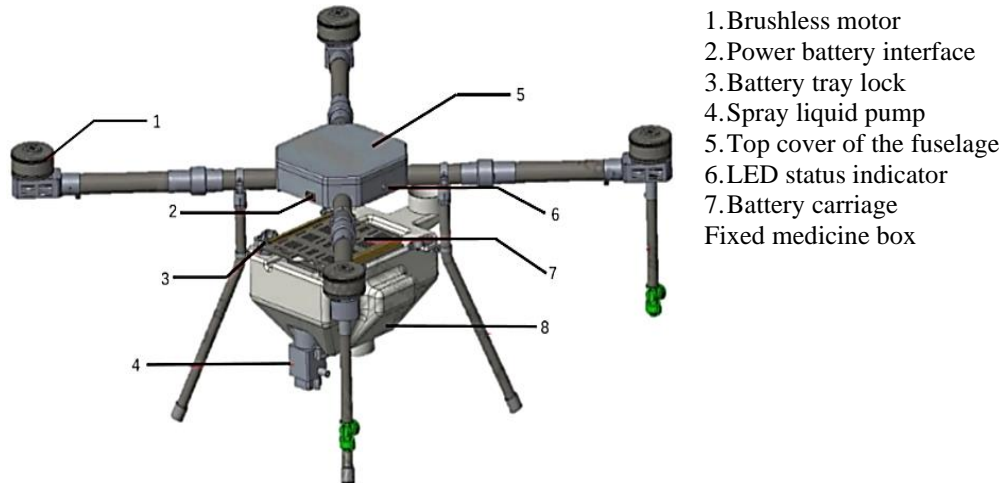


Figure 5. AX-1000 UAV fuselage structure diagram

Table 3. Power meter parameters

Model	Mass (g)	Voltage range/accuracy	Current range/accuracy	Power accuracy
ZET-8	129 g	4.5-150 V/0.1 V	0-150 A/0.1 A	0.1 W

3.4. Verification experiment

The test was carried out on the lawn next to the lotus garden in Qilin District, South China Agricultural University, Guangzhou City, Guangdong Province on September 16, 2021. During this period, the ambient temperature was approximately 30 degrees, and the ground wind was Level 1, which satisfies the flight test conditions. The test flight before the test is shown in Figure 6.



Figure 6. Preparation before the UAV experiment

After completing the UAV configuration according to the corresponding parameters of the verification point, the curve power meter is connected to the power battery. In the GPS flight mode, the UAV is controlled to hover stably for 5 minutes, and the curve power meter will record the power change data throughout the journey. To avoid data loss, after each landing, the power meter data are uploaded to the computer before performing the next experiment. The entire verification experiment contains 7 verification points, and each verification point needs to complete three repeated tests, for a total of 21 tests. The final experimental data are shown in Table 4.

Table 4. Endurance cut-off line verification results

	Sampling point	Battery mass (kg)	Payload (kg)	Test1 (h)	Test2 (h)	Test3 (h)	Theoretical value (h)	Average error rate
Conclusion ①	#1	4	3	0.528	0.530	0.531	0.562	5.69%
	#2	3	4	0.397	0.395	0.396	0.414	4.18%
	#3	2	5	0.265	0.263	0.262	0.270	2.50%
Conclusion ②	#2	3	4	0.397	0.395	0.396	0.414	4.18%
	#4	3.57	5	0.399	0.397	0.397	0.411	3.25%
	#5	10	0	0.958	0.962	0.963	1.004	4.33%
Conclusion ③	#6	10.5	0	0.987	0.985	0.986	1.005	1.89%
	#7	11	0	0.971	0.969	0.971	1.002	3.19%

3.5. Experimental results and analysis

According to the data of Verification Points 1, 2, and 3, when the mass of the battery increases from 2 kg to 3 kg and 4 kg, the mass ratio increases by 50% and 100%, respectively. Correspondingly, the average endurance increases from 0.263 h to 0.396 h and 0.53 h. The endurance improvement rates are 50.57% and 101.52%, respectively. Thus, Conclusion 1 is proved. From the data of Verification Points 2 and 4, it can be seen that when the battery mass increases by 0.57 kg and the payload increases by 1 kg, the average endurance time is basically unchanged, and both are 0.4 h. Thus, conclusion 2 is proved. From the data of verification points 5, 6, and 7, it can be seen that without a payload, the battery mass corresponding to the turning point of the endurance curve is 10.5 kg. When the mass of the battery increases by 0.5 kg, the average endurance time drops from 0.986 h to 0.97 h, and the three conclusions are proven.

In addition, from the data in Table 4, it can be seen that the average error rate distribution range of the verification points is 1.89% to 5.69%, and the overall accuracy of the theoretical model reaches a relatively high level, which meets the requirements of actual engineering applications.

4. RESULTS AND DISCUSSION

The current configuration regularity is suitable for different brands and different structural layouts of rotary-wing transport UAVs. After obtaining the parameters of the specific model, the endurance time configuration zone map can be quickly constructed to analyze and evaluate the current drone's endurance capabilities. Targeted optimization suggestions are given based on the evaluation results. To demonstrate the practical application value of the abovementioned model regularity, four models with high utilization rates in the transport UAVs market are taken as the evaluation objects. The detailed configuration parameters are shown in Table 5. The expression of the pull-power fitting function of the supporting power motors of each model is (9). The corresponding fitting function coefficients are shown in Table 6.

$$P_T = k_1 T^2 + k_2 T + k_3 \quad (9)$$

Table 5. Performance parameters of the main models

Serial number	Model	Motor	Propeller	Aircraft mass (kg)	Standard payload (kg)	Standard battery (kg)	Endurance time (min)	Model output (min)
UAV1	MG1p	6010	21*5.7	9.8	10	4	9	8.48
UAV2	"baye"	C8017	30*8	22	20	5.1	8.5	8.1
UAV3	TAX16	M10	28*8	16	16	5.1	12	11.52
UAV4	TP32	T15	30*99	25	32	9.7	8	9

Table 6. Power motor tension-power fitting coefficient table

Serial number	Motor	k1	k2	k3	R-square
UAV1	DJI6010	21.34	60.13	-2.147	0.9999
UAV2	C8017	9.802	92.5	-43.18	0.9997
UAV3	M10	10.45	60.61	-3.339	0.9996
UAV4	T15	7.961	13	186.2	0.9956

Table 5 shows that the current endurance model has a good application effect, and its output is basically consistent with the manufacturer's endurance data. However, due to model errors and the inconsistent endurance test standards of various manufacturers, there is still an error of 5% to 12.5% between the two models. Substituting the parameters of each UAV into the model, the drawn endurance time zone evaluation chart is shown in Figures 7(a) to 7(d).

Figure 7 shows that the standard operating configuration points of the above models are all located in the ideal configuration area. Among them, Figure 7(a) shows that the operating point of UAV1 is close to

the cut-off zone, which almost maximizes the performance of the UAV. In Figure 7(b), the operating point of UAV2 is located inside the ideal configuration area, taking into account the endurance and reliability of the UAV, and the overall operating efficiency has reached a relatively high level. Figure 7(c) shows that the operating point of UAV3 is located at the edge of the ideal configuration area, and there is room for improvement in the overall performance. If a 1 kg payload and 1 kg battery mass are added at the same time, the endurance time will be increased from 0.187 h to 0.201 h, and the endurance time improvement rate is 6.97%. Figure 7(d) shows that The operating configuration point of UAV4 is located in the light-load configuration area, which has great potential for improvement. If the battery and payload are increased by 2 kg at the same time, the endurance time will be increased from 0.242 h to 0.265 h, the endurance time improvement rate is 9.5%, and the overall operating efficiency of the machine will be greatly improved.

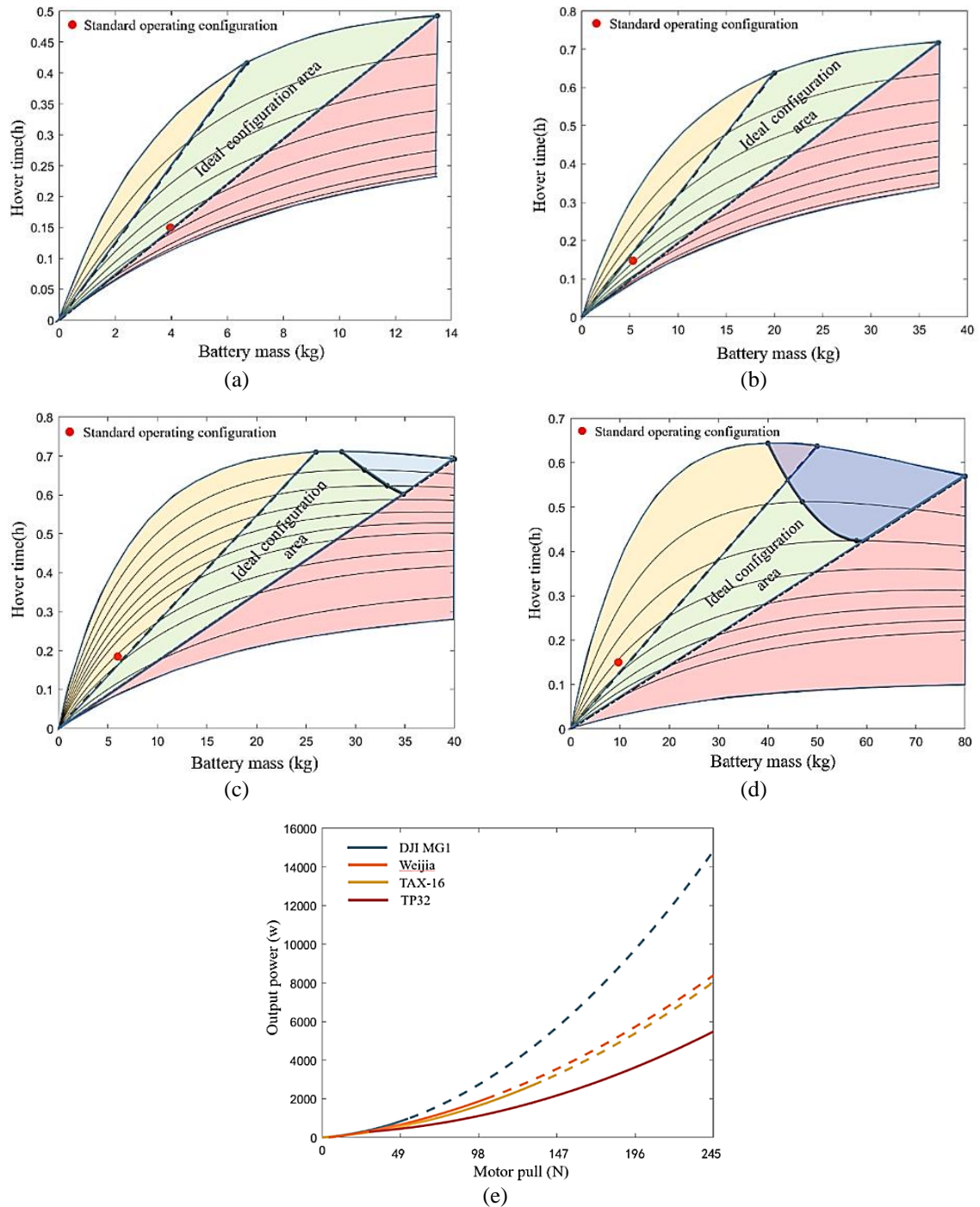


Figure 7. The endurance evaluation chart of each model (a) UAV1, (b) UAV2, (c) UAV3, (d) UAV4, (e) UAV1-UAV4

Comparing the endurance evaluation charts of various models, it can be seen that as the load capacity of the UAV increases, the ideal configuration area gradually shifts from the light load to the heavy load area, and the endurance saturation area gradually expands. Through (2), it can be seen that the shape of the endurance curve is mainly affected by the performance of the motor. Based on this, the motor pull-power fitting curves of the four models are drawn, and the results are shown in Figure 7(e). Figure 7 shows that the standard motor of UAV4 has the highest pull force and the lowest slope of the corresponding pull force-power fitting curve. The power consumption of this motor increases slowly during the pull force growth process, and it is suitable for working in the high-pull force region of the motor curve. The area corresponding to the ideal configuration is biased toward the high-load area. The UAV1 standard motor has a small pull force, and power consumption increases rapidly during the process of an increasing pull force. It is suitable for working in the low-pull area of the tensile curve, and the ideal configuration area is biased toward the low-load area. Otherwise, its energy consumption economy will be significantly reduced. In addition, high-load models such as UAV3 and UAV4 have a large configuration change range. After reaching the turning point of the endurance curve, there is still a certain amount of load configuration space. Therefore, the endurance saturation area in the corresponding endurance evaluation chart is larger. The low-load capacity of UAV1 is poor, and the ultimate load capacity often does not reach the load configuration required for the turning point of the endurance curve. Thus, the endurance saturation zone will not appear in the corresponding endurance evaluation chart.

The standard operation configuration points in the above endurance evaluation chart only represent the endurance status of the drone when hovering. In the actual flight process, to maintain the flying height, the motor pulling force will increase with the increase in the inclination angle of the body, corresponding to the motor pulling force. The working point of the power curve is correspondingly increased, which is equivalent to an increase in the payload and will eventually cause the working configuration point to shift along the output power coordinate axis to the load cut-off zone. If the load configuration is too high at this time, the operation configuration point moves to the load cut-off area, which may result in insufficient power of the UAV and cause a crash.

5. CONCLUSION

This article focuses on rotor transport drones, developing a hover model based on an analysis of endurance factors and validating the model's reliability through practical testing. The study combines different load configuration intervals with the model to establish the optimal endurance configuration regularity, which is then used to evaluate the battery life of several mainstream transport drones. The key findings of this research offer valuable insights into drone configuration and operational efficiency.

The primary findings reveal that when the AX-1000 UAV is tested with a 10.5 kg battery configuration, its battery life reaches the peak value of 0.99 hours. Any increase or decrease in battery size results in a reduced battery life, illustrating the delicate balance required in battery sizing to optimize performance. Additionally, the paper introduces a theoretical model for calculating hover endurance time, considering the impact of UAV distribution, hover energy consumption, and endurance. The model, developed through data testing and curve fitting, demonstrates high predictive accuracy, with an error rate ranging from 1.89% to 5.69%. This model is applicable to transport drones of varying sizes and rotor quantities, allowing for rapid calculations of battery life and payload mass, thus offering valuable guidance for operational decision-making.

The research also innovates by introducing the concepts of pulling redundancy and load cutoff lines into the evaluation of battery life. It classifies operational parameters into light-load/ideal configuration areas, battery life, and load deadlines. In the light-load configuration area, drones exhibit long battery life due to low operational loads, making them suitable for applications like remote sensing. The ideal configuration area, however, optimally balances load and battery life, ensuring the best performance for heavy-load transport drones. The load deadline marks the point beyond which further increases in load exceed the drone's capacity, providing no practical benefits. This classification method not only clarifies the load-endurance relationship but also aids in selecting the most efficient power configuration during both the design and operational stages. By comparing endurance partition diagrams for different power configurations, optimal configurations can be quickly identified to enhance drone performance.

Further optimization results show that the operational configurations of UAV1 and UAV2 are already ideal, while UAV3 and UAV4 could benefit from adjustments. Specifically, increasing the operating load of UAV3 by 6.25% results in a 6.97% increase in battery life, and a similar increase for UAV4 yields a 9.5% improvement. These findings highlight how optimal endurance configuration regularity can be effectively applied to real-world drone models, offering targeted solutions for improving battery life and operational efficiency, ultimately leading to higher economic returns.

The study also observes that as the motor's maximum tensile force increases, the ideal configuration area shifts from the light-load to the heavy-load configuration area. This shift suggests that when large motors operate in the high-pull area, overall efficiency improves. Consequently, future research on transport drones is expected to focus more on large-scale and overloaded structures to meet higher load and endurance requirements while improving power efficiency.

In conclusion, the endurance time model and optimal endurance configuration regularity proposed in this study offer an initial solution to the challenge of configuring operational parameters for transport UAVs. This approach provides a scientifically grounded framework for evaluating and optimizing drone performance. Looking ahead, the next phase of research will focus on developing a dynamic endurance model that incorporates dynamic energy consumption during flight. This expanded model, combined with emerging technologies such as intelligent route planning and precise spraying, promises to further enhance the performance and efficiency of transport UAVs, contributing significantly to their optimization.

ACKNOWLEDGEMENTS

This work is supported by Guangdong Basic and Applied Basic Research Foundation under Grant 2023A1515011932 and in part by the Key Technologies Research and Development Program of Guangzhou under Grant 202206010164 and Grant 2023B03J1323, China.




REFERENCES

- [1] F. Ahmed, J. C. Mohanta, A. Keshari, and P. S. Yadav, "Recent advances in unmanned aerial vehicles: A review," *Arabian Journal for Science and Engineering*, vol. 47, no. 7, pp. 7963–7984, Apr. 2022, doi: 10.1007/s13369-022-06738-0.
- [2] I. A. Shah, A. Laraib, H. Ashraf, and F. Hussain, "Drone technology: Current challenges and opportunities," in *Cybersecurity Issues and Challenges in the Drone Industry*, IGI Global, 2024, pp. 343–361. doi: 10.4018/979-8-3693-0774-8.ch014.
- [3] J. Li *et al.*, "Rapid evaluation model of endurance performance and its application for agricultural UAVs," *Drones*, vol. 6, no. 8, p. 186, Jul. 2022, doi: 10.3390/drones6080186.
- [4] N. Elmeseiry, N. Alshaer, and T. Ismail, "A detailed survey and future directions of unmanned aerial vehicles (UAVs) with potential applications," *Aerospace*, vol. 8, no. 12, p. 363, Nov. 2021, doi: 10.3390/aerospace8120363.
- [5] Y. Lu *et al.*, "Precision fertilization and irrigation: Progress and applications," *AgriEngineering*, vol. 4, no. 3, pp. 626–655, Jul. 2022, doi: 10.3390/agriengineering4030041.
- [6] H. A. Langåker *et al.*, "An autonomous drone-based system for inspection of electrical substations," *International Journal of Advanced Robotic Systems*, vol. 18, no. 2, Mar. 2021, doi: 10.1177/17298814211002973.
- [7] L. Qian, S. Graham, and H. H. T. Liu, "Guidance and control law design for a slung payload in autonomous landing: A drone delivery case study," *IEEE/ASME Transactions on Mechatronics*, vol. 25, no. 4, pp. 1773–1782, Aug. 2020, doi: 10.1109/TMECH.2020.2998718.
- [8] J. Li, Y. Zhan, F. Ouyang, Y. Li, and Y. Lan, "Optimization of rotor spacing and energy consumption test of multi-wing single-arm longitudinal layout electric UAV," (In Chinese: 多翼单臂纵列式布局电动无人机旋翼间距优化及能耗试验) *Trans. Chinese Soc. Agric. Eng.*, vol. 35, no. 23, pp. 87–95, Nov. 2019, doi: 10.11975/j.issn.1002-6819.2019.23.011.
- [9] L. Yang, "Numerical simulation and optimization research on aerodynamic characteristics of longitudinal six-rotor heavy-load UAV," (In Chinese: 纵列式六旋翼大载荷无人机气动特性数值模拟及其优化研究) Jilin Univ., 2015.
- [10] L. Zhang and Z. Xie, "Performance calculation and analysis of propellers for electric multirotor UAVs," (In Chinese: 电动多旋翼无人机螺旋桨的性能计算与分析) *Sci. Technol. Innov. Appl.*, no. 01, pp. 17–18, Jan. 2016, doi:10.19981/j.cn23-1581/g3.2016.01.008.
- [11] F. Liu and X. Ma, "Research on improving endurance performance of small electric UAVs," *Flight Mech.*, vol. 28, no. 05, pp. 13–15, May 2010, doi:10.13645/j.cnki.f.d.2010.05.020.
- [12] Y. Zhang and R. Liu, "Design of a new type of hexacopter," (In Chinese: 一种新型六旋翼飞行器的设计) *Mech. Electron. Eng.*, no. 05, pp. 64–66, May 2010.
- [13] D. Duan, J. Pei, R. Zu, and J. Li, "Power optimization control of motor-variable-pitch propeller power system," *Acta Aeronautica et Astronautica Sinica*, vol. 42, no. 03, pp. 80–91, Mar. 2021, doi: 10.7527/S1000-6893.2020.23933.
- [14] M. Rinaldi, S. Primates, and G. Guglieri, "A comparative study for control of quadrotor UAVs," in *Applied Sciences (Switzerland)*, vol. 13, no. 6, MDPI AG, 2023, p. 3464. doi: 10.3390/app13063464.
- [15] L. Wang, M. Xu, Q. Hou, Z. Wang, Y. Lan, and S. Wang, "Numerical verification on influence of multi-feature parameters to the downwash airflow field and operation effect of a six-rotor agricultural UAV in flight," *Computers and Electronics in Agriculture*, vol. 190, p. 106425, Nov. 2021, doi: 10.1016/j.compag.2021.106425.
- [16] H. Li, H. Zhu, Z. Jiang, and Y. Lan, "Performance characterization on downwash flow and spray drift of multirotor unmanned agricultural aircraft system based on CFD," *International Journal of Agricultural and Biological Engineering*, vol. 15, no. 3, pp. 1–8, 2022, doi: 10.25165/j.ijabe.20221503.7315.
- [17] H. Zhang, B. Song, F. Li, and J. Xuan, "Multidisciplinary design optimization of an electric propulsion system of a hybrid UAV considering wind disturbance rejection capability in the quadrotor mode," *Aerospace Science and Technology*, vol. 110, p. 106372, Mar. 2021, doi: 10.1016/j.ast.2020.106372.
- [18] X. Ji, "Research on energy consumption optimization path planning method of rotorcraft UAV with multi-feature fusion," (In Chinese: 多特征融合的旋翼无人机能耗优化路径规划方法研究) M.S. thesis, Northwest Univ., 2021, doi: 10.27405/d.cnki.gxbdu.2021.000001.
- [19] J. Li, H. Luo, C. Zhu, *et al.*, "Research on combined algorithm of UAV spraying planning based on energy optimization," (In Chinese: 基于能量优化的无人机喷施规划组合算法研究) *Trans. Chinese Soc. Agric. Mach.*, vol. 50, no. 10, pp. 10, Oct. 2019.
- [20] G. Yang, "Research on dynamic performance and configuration optimization of fuel cell UAV power supply system," (In Chinese: 燃料电池无人机电源系统的动态性能及配置优化研究) M.S. thesis, Dept. Elect. Eng., Univ. Electronic Sci. and




- Technol. of China, Chengdu, China, 2021, doi: 10.27005/d.cnki.gdzku.2021.001227.
- [21] B. CHEN, L. ZHENG, X. LI, Y. FENG, Z. XU, and Z. DAI, "Discharge performance and charge-discharge heat generation characteristics of aging batteries," *Energy Storage Science and Technology*, vol. 11, no. 2, p. 679, 2022.
- [22] L. Mariga, I. Silva Tiburcio, C. A. Martins, A. N. Almeida Prado, and C. Nascimento, "Measuring battery discharge characteristics for accurate UAV endurance estimation," *The Aeronautical Journal*, vol. 124, no. 1277, pp. 1099–1113, 2020. doi:10.1017/aer.2020.16
- [23] D. Y. Tang, M. T. Gong, J. S. Yu, and X. Li, "A power transfer model-based method for lithium-ion battery discharge time prediction of electric rotatory-wing UAV," *Microelectronics Reliability*, vol. 114, p. 113832, Nov. 2020, doi: 10.1016/j.microrel.2020.113832.
- [24] X. Zhang, S. Wu, and N. Li, "Research on optimization and strategy of lithium battery energy management system," (In Chinese: 锂电池能量管理系统优化与策略研究) *s*, no. 04, pp. 24–26, Apr. 2021.
- [25] L. Bauersfeld and D. Scaramuzza, "Range, endurance, and optimal speed estimates for multicopters," *IEEE Robotics and Automation Letters*, vol. 7, no. 2, pp. 2953–2960, Apr. 2022, doi: 10.1109/LRA.2022.3145063.
- [26] K. Hectors and W. De Waele, "Cumulative damage and life prediction models for high-cycle fatigue of metals: A review," *Metals*, vol. 11, no. 2, pp. 1–32, Jan. 2021, doi: 10.3390/met11020204.
- [27] S. S. Kadam and S. Umale, "Effect of various fin geometries on heat dissipation of traction motors used in Electric vehicles," *Journal of Physics: Conference Series*, vol. 2007, no. 1, p. 12021, Aug. 2021, doi: 10.1088/1742-6596/2007/1/012021.

BIOGRAPHIES OF AUTHORS






Huang Zihan    primary research focuses on the payload and endurance of rotary-wing UAVs, obstacle avoidance technology for agricultural UAVs, binocular stereo vision recognition, and robot control technology. He is dedicated to enhancing the payload capacity and endurance of UAVs, developing efficient obstacle avoidance systems for agricultural UAVs, utilizing binocular stereo vision technology for precise object recognition, and optimizing robot control algorithms to improve the efficiency of automated operations. He can be contacted at zihan494830@163.com.



Long Bo    received master's degree from South China Agricultural University in 2022. Focusing on the effect and efficiency of precise operation of rotary-wing UAVs, configuring UAV energy, load, and architecture, exploring the operation performance of large-load UAVs, explore the relationship between energy consumption and operational performance of drones, construct a drone endurance time model, and achieve maximum efficiency in agricultural drone operations, and planning crop characteristics precise spraying plan. He can be contacted at 496003608@qq.com.



Li Jiyu    received Ph.D. degree from South China Agricultural University in 2014. Currently, he is a professor and doctoral supervisor at the College of Engineering. And he is editorial board member of "agriculture", young editorial board member of "Journal of Agricultural Machinery". Focusing on the effect and efficiency of precise operation of rotary-wing UAVs, developing the new field and airborne sensors, developing airflow target flight control systems, configuring UAV energy, load, and architecture, exploring the operation performance of large-load UAVs, and planning crop characteristics precise spraying plan. He can be contacted at lijyu@scau.edu.cn.